Magnetic transitions in double perovskite $Sr_2FeRe_{1-x}Sb_xO_6$ ($0 \leqslant x \leqslant 0.9$)

Alexandra Jung,[1] Vadim Ksenofontov,[1] Sergey Reiman,[1] Helen Annal Therese,[1] Ute Kolb,[2] Claudia Felser,[1] and Wolfgang Tremel[1]

[1]*Institut für Anorganische und Analytische Chemie, Johannes Gutenberg-Universität Mainz, D-55099 Mainz, Germany*

[2]*Institut für Physikalische Chemie, Johannes Gutenberg-Universität Mainz, D-55099 Mainz, Germany*

(Received 25 August 2005; revised manuscript received 16 December 2005; published 13 April 2006)

The double perovskites Sr_2FeMO_6 (M=Re,Mo) belong to the important class of half-metallic magnetic materials. In this study we explore the effect of replacing the electronic 5*d* buffer element Re with variable valency by the main group element Sb with fixed valency. X-ray diffraction reveals $Sr_2FeRe_{1-x}Sb_xO_6$ ($0 < x < 0.9$) to crystallize without antisite disorder in the tetragonally distorted perovskite structure (space group $I4/mmm$). The ferrimagnetic behavior of the parent compound Sr_2FeReO_6 changes to antiferromagnetic upon Sb substitution as was determined by magnetic susceptibility measurements. Samples up to a doping level of 0.3 are ferrimagnetic, while Sb contents higher than 0.6 result in an overall antiferromagnetic behavior. ^{57}Fe and ^{121}Sb Mössbauer spectroscopy specifies the valence state of Sb to be +5 within the whole range of substitution whereas the Fe valence state changes from +2.7 for the parent compound to +2.9 for $Sr_2FeRe_{0.1}Sb_{0.9}O_6$. Accordingly, Fe adopts the role of an electronic buffer element from Re upon heavy Sb doping. Additionally, ^{57}Fe Mössbauer results show a coexistence of ferri- and antiferromagnetic clusters within the same perovskite-type crystal structure in the Sb substitution range $0.3 < x < 0.8$, whereas Sr_2FeReO_6 and $Sr_2FeRe_{0.9}Sb_{0.1}O_6$ are "purely" ferrimagnetic and $Sr_2FeRe_{0.1}Sb_{0.9}O_6$ contains antiferromagnetically ordered Fe sites only. Consequently, a replacement of the Re atoms by a nonmagnetic main group element such as Sb blocks the superexchange pathways -Fe-O-Re(Sb)-O-Fe- along the crystallographic axis of the perovskite unit cell and destroys the itinerant magnetism of the parent compound.

DOI: 10.1103/PhysRevB.73.144414 PACS number(s): 75.50.Cc, 82.80.Ej, 71.20.−b, 72.25.Ba

I. INTRODUCTION

The double perovskites Sr_2FeReO_6 and Sr_2FeMoO_6 reveal half-metallic ferrimagnetic behavior at room temperature. Both compounds obey a relatively high Curie temperature (401 K and 415 K, respectively) which is an important condition for a high degree of spin polarization at room temperature. The conceptual basis for half-metallic ferromagnetism is a large density of states of one spin direction at the Fermi level whilst the other spin direction is insulating. The origin of the large density of states in the vicinity of the Fermi level can be related to a van Hove singularity in the band structure of these compounds as it was suggested in a previous study.[1] It could be demonstrated by the systematic use of electronic band structure calculations that it is possible to predict and tune the electronic structure of spintronic materials, e.g., by diamagnetic dilution[2–5] (i.e., systematic replacement of ions contributing to the magnetic interactions within the sample by diamagnetic ions) of the Fe-sublattice by Zn^{2+} which leads to a transition of the magnetic properties from ferrimagnetic for slight Zn-doping (up to 60%) to ferromagnetic for heavy Zn-doping (>60%). This conclusion was drawn from the weak overall concentrational dependence of the paramagnetic Curie temperature in the solid solution series $Sr_2Fe_{1-x}Zn_xReO_6$ ($0 < x < 0.9$) which is compatible with itinerant magnetic behavior. With increasing Zn concentration the exchange interaction within the Fe based sublattice weakens. At some critical concentration of Zn ($x \cong 0.6-0.8$) the long-range magnetic correlations within this sublattice disappear, whereas the long-range magnetic correlations within the Re sublattice remain unchanged. Therefore, heavy Zn dilution leads to the transformation of the ferrimagnetic to the ferromagnetic type of ordering.[1]

Sr_2FeReO_6 as well as Sr_2FeMoO_6 belong to the family of double perovskites of the general formula $A_2MM'O_6$, where the M and M' sites are occupied alternatively by different transition metal cations (M=first row transition metal; M'=Mo,W,Re).[6,7] The ideal structure of these compounds can be viewed as a regular arrangement of corner sharing MO_6 and $M'O_6$ octahedra alternating along the three directions of the crystal with large A cations situated in the voids between the octahedra (Fig. 1). Crystal structure and physical properties of double perovskite oxides strongly depend on size and valencies of the cations A, M and M'. For example, Sr_2FeReO_6 as well as Sr_2FeMoO_6 show a slight tetragonal distortion from the ideal cubic structure.[8] Sr_2FeReO_6 crystallizes in the space group $I4/mmm$ as determined by x-ray powder diffraction [Fig. 2(a)]. Cations Fe^{3+} ($3d^5$, $S=5/2$) and Re^{5+} ($5d^2$, $S=1$) order antiferromagnetically and the conduction band is composed of the 5*d* down spin electrons of Re^{5+}. The resulting arrangement of Fe^{3+} and Re^{5+} leads to an overall ferrimagnetic behavior of Sr_2FeReO_6.[9–12]

In Ref. 1 it turned out that the 5*d* transition element Re plays an important role in the magnetic coupling between the 3*d* metal atoms. Furthermore, the 5*d* elements act as an electron buffer which stabilizes the valence state of the magnetic element Fe, independent of the doping level. In the present study we explore the alternative approach to replace the electronic 5*d* buffer element Re by the main group element Sb which formally has the same oxidation state as Re and Mo in the double perovskites Sr_2FeReO_6 and Sr_2FeMoO_6. One can envision that the lack of *d* orbitals requires a fixed valence for Sb and prevents Sb to act as an electron buffer. Further-

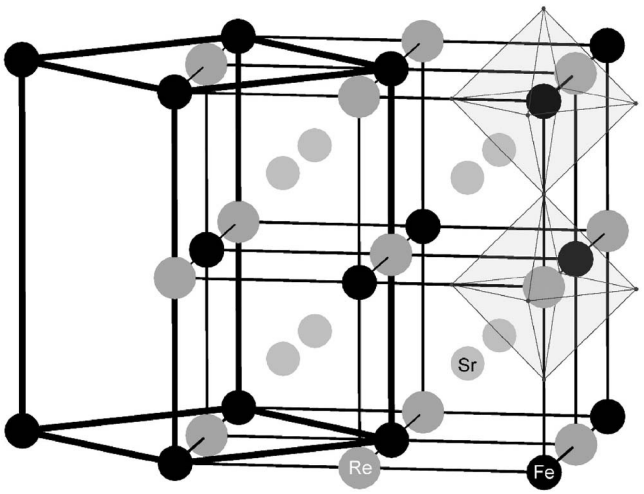

FIG. 1. Crystal structure of the double perovskite Sr_2FeReO_6; Fe (black), Re (dark grey), Sr (light grey), and O (octahedra); the cubic lattice is drawn in thin black lines, the tetragonal lattice in thick black lines.

more, we expect that the lack of *d* orbitals should have a dramatic influence on the superexchange between the magnetic atoms through the Re *d* orbitals.

In an attempt to probe the influence of the diamagnetic dilution of the Re sublattice we have investigated the solid solution series $Sr_2FeRe_{1-x}Sb_xO_6$ $(0<x<0.9)$. Here, we report the synthesis, crystal structure and magnetic properties of these compounds.

II. EXPERIMENT

Starting materials were reagent grade SrO (Aldrich, 99.9% purity), Fe_2O_3 (Alfa Aesar, 99.99% purity), Re metal, Re_2O_7 (Alfa Aesar, 99.9% purity), and Sb_2O_5 (Alfa Aesar, 99.999% purity). All starting materials are stored under argon (Braun Labmaster) and examined by x-ray powder diffraction before use.

The $Sr_2FeRe_{1-x}Sb_xO_6$ $(0\leqslant x\leqslant 0.9)$ samples were prepared by high-temperature solid state reactions. Because of the strongly hygroscopic properties of SrO and the high vapor pressure of Re_2O_7 the samples were prepared under inert gas atmosphere in a glove box. Stoichiometric amounts of SrO, Fe_2O_3, Re, Re_2O_7, and Sb_2O_5 $[2\ SrO:(1-x)/2\ Fe_2O_3:0.3\ Re:0.35\ Re_2O_7:x/2\ Sb_2O_5]$ were ground in an agate mortar and pressed into pellets. In order to avoid Sr attack on the quartz tubes these pellets were transferred into corundum containers and finally sealed in evacuated quartz glass tubes. The samples were annealed for seven days at 1000 °C. Thereafter they were rapidly cooled to room temperature by quenching in ice. Preparations aiming at the fully substituted compound Sr_2FeSbO_6 were unsuccessful.

X-ray powder diffraction measurements were performed using a Seifert XRD 3000 TT diffractometer with a secondary monochromator (Si) equipped with a Cu source and operating in reflection mode and a Bruker D5000 with a secondary monochromator (graphite) equipped with a Co source and operating in reflection mode.

HRTEM analyses were measured by FEI Tecnai F30 ST operated at an extraction voltage of 300 kV (equipped with an EDXA energy dispersive x-ray spectrometer) and by selected area electron diffraction techniques (SAED). For transmission electron microscopic (TEM) studies, the sample was dispersed in ethanol ultrasonically first and then a drop of it was placed on a copper grid coated with a carbon film.

The variable-temperature magnetic susceptibility measurements of $Sr_2FeRe_{1-x}Sb_xO_6$ were performed using the Quantum Design MPMS-XL SQUID magnetometer, equipped with a high-temperature furnace. Experimental data were corrected for diamagnetism using Pascal's constants.[13]

The dc conductivity measurements were done using the four point probe method. The samples were measured using an OXFORD helium bath cryostat operating in the temperature range from 4.2 K to 295 K.

Mössbauer measurements of $Sr_2FeRe_{1-x}Sb_xO_6$ powder samples were performed in transmission geometry using a constant-acceleration spectrometer and a helium bath cryostat. ^{57}Fe Mössbauer spectra were recorded between room temperature and 4.2 K using the 50 mCi source ^{57}Co(Rh). The Recoil 1.03 Mössbauer Analysis Software was used to fit the experimental spectra.[14] Isomer shift values are quoted relative α-Fe at 293 K.

A ^{121m}Sn $(CaSnO_3)$ source with activity of 3.0 mCi was placed together with the absorber in the helium bath cryostat. ^{121}Sb Mössbauer spectra were analyzed with the program EFFINO (Ref. 15) using Lorentzian line shapes. During the fit

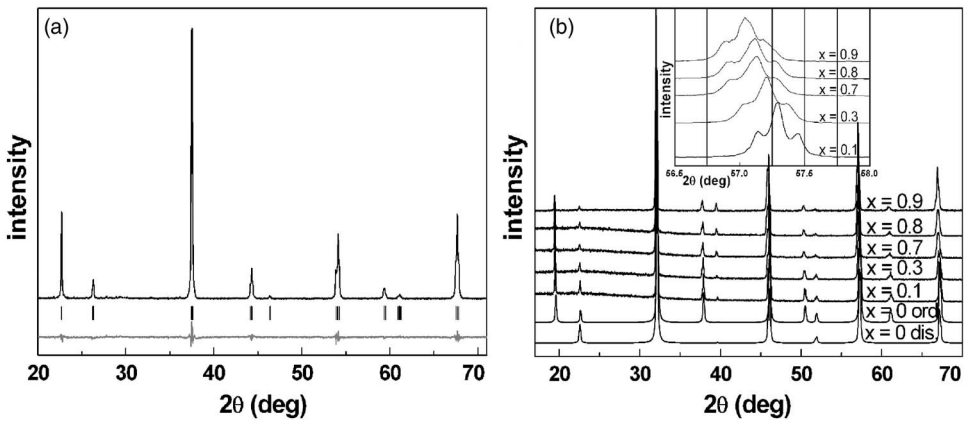

FIG. 2. (a) X-ray pattern of Sr_2FeReO_6 (black), positions of the reflections (black bars), and the corresponding difference curve (grey); (b) calculated x-ray pattern of Sr_2FeReO_6 in space group $I4/mmm$ with fully disordered Fe/Re site ($x=0$ dis.), with fully ordered Fe/Re site ($x=0$ ord.) and measured x-ray patterns of $Sr_2FeRe_{1-x}Sb_xO_6$; inset: range $56.5°<2\theta<58.0°$ highlighted.

the source recoil-free fraction value was fixed at 0.6.

Band structure calculations were performed within the potential augmented plane-wave (FLAPW) framework within the generalized gradient approximation (GGA).[16] The crystal structure of the parent compound Sr_2FeReO_6 was approximated by the ideal cubic structure of a double perovskite with the lattice parameter $a=7.89$ Å. The number of k points in the irreducible Brillouin zone is 20. The crystal structure of Sr_2FeSbO_6 was approximated from the crystal structures of $Sr_2FeRe_{0.2}Sb_{0.8}O_6$ and $Sr_2FeRe_{0.1}Sb_{0.9}O_6$ to be tetragonal (space group $I4/mmm$) with lattice parameters $a=5.57$ Å and $c=7.94$ Å. The number of k-points in the irreducible Brillouin zone is 28. The convergence criterion was fixed to 0.0001 Ry for both calculations.

III. RESULTS

A. Structural characterization

The crystal structures of the series $Sr_2FeRe_{1-x}Sb_xO_6$ ($0 \leqslant x \leqslant 0.9$) were determined by powder x-ray diffraction in the reflection mode. The corresponding x-ray patterns reveal that the samples—as the undoped parent compounds—adopt a double perovskite structure.[6,7,17,18] An x-ray pattern of Sr_2FeReO_6 together with the Rietveld fit (refined with the FULLPROF program[19]) and the corresponding difference curve are given in Fig. 2(a). X-ray patterns of $Sr_2FeRe_{1-x}Sb_xO_6$ are presented in Fig. 2(b) together with the most informative part of the x-ray diffractogram in the range $56.5° < 2\theta < 58.0°$ which is highlighted as an insert in the figure. The reflection profiles indicate that the symmetry of the lattice does not change as a function of the Sb content. The three elements Fe, Re, and Sb have to be distributed on two lattice sites which raises the question of cation disorder. Attempts to account for an Fe/Re antisite disorder with the aid of Rietveld refinement lead to maximum disorder ratios of 2% independent of the degree of Sb doping. These findings are supported by the results of the high resolution transmission electron microscopy (HRTEM) studies (*vide infra*). The observed absence of antisite disorder precludes the presence of -Fe-O-Fe- clusters. Lattice parameters a and c of Sr_2FeReO_6 and $Sr_2FeRe_{1-x}Sb_xO_6$ as obtained by Rietveld refinements are plotted in Fig. 3. As predicted by Vegard's rule the dependence of the lattice parameters on the "doping level" (i.e., the Sb content of the solid solution) is almost linear, confirming the existence of a continuous solid solution series in the range $0 \leqslant x \leqslant 0.9$. The lattice parameters and unit cell volumes increase with increasing Sb content as illustrated in Figs. 3(a) and 3(b). The increase of the cell volume can be explained from the ionic radii of Re^{5+} and Sb^{5+} [$r(Re^{5+}) = 58$ pm, $r(Sb^{5+}) = 60$ pm].[20]

The extent of the tetragonal distortion from the ideal cubic structure can be visualized by plotting the ratio of the tetragonal lattice parameters c/a as a function of the degree of substitution [Fig. 3(b)]. The condition for a cubic cell is a c/a ratio of $\sqrt{2}$. A deviation from cubic symmetry leads to a change of the c/a ratio. A c/a ratio of 1.421 observed for members of the series $Sr_2FeRe_{1-x}Sb_xO_6$ does not show any significant dependence on the doping level and is indicative of a tetragonal distortion.

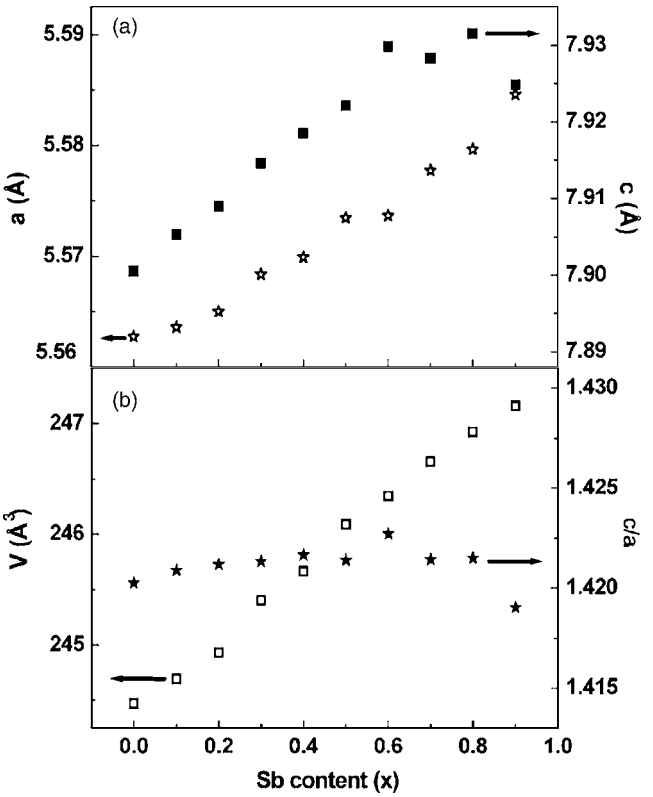

FIG. 3. (a) Lattice parameters a (☆) and c (■) of the tetragonal unit cell and (b) volume per unit cell (□) and lattice parameter relation c/a (⋆) versus Sb content.

The above results qualitatively agree with the structural behavior expected from an analysis of the tolerance factor t for perovskites of the general formula AMX_3, where the ionic radii were taken from Shannon.[20] The tolerance factor describes the interrelation between the perovskite structure and the associated ionic radii,[21,22]

$$t = \frac{r(A) + r(X)}{\sqrt{2}[r(M) + r(X)]}.$$

To point out the concentrational dependence of the tolerance factor, one should know the valence state of the ions in the crystal structure. The valence states of iron and antimony are important because the ionic radii of Fe^{2+} and Fe^{3+} and Sb^{3+} and Sb^{5+} which appear in the above equation, differ significantly, whereas the ionic radius of Re is practically valence independent. The following results of a detailed study of the iron and antimony valence states by means of ^{57}Fe and ^{121}Sb Mössbauer spectroscopy (discussed in detail below) are used to calculate the perovskite tolerance factor t for the substitution series: the antimony valence state remains constant at $+5$ for the whole substitution range, whereas the iron valence state changes from $Fe^{2.7+}$ for the parent compound to $Fe^{2.9+}$ for $Sr_2FeRe_{0.1}Sb_{0.9}O_6$.

To determine t for the whole substitution range, one has to consider two different effects. First, the replacement of Re by Sb^{5+} forces the tolerance factor to decrease slightly from 0.896 to 0.890. However, this first effect is overcompensated by a second effect, the change of the iron valence state from

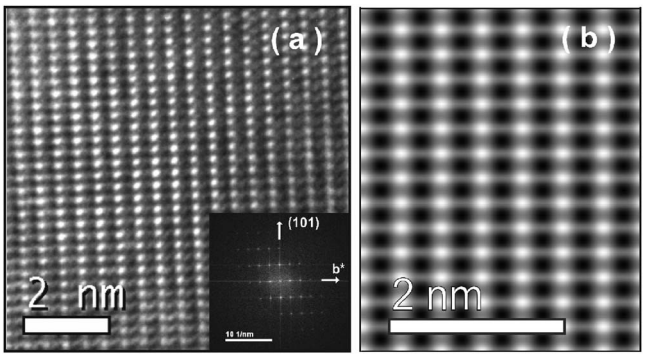

FIG. 4. Experimental high resolution transmission electron micrograph, inset: (b) image of zone [1 0 −1] simulated by the multislice method (Refs. 23 and 24).

+2.7 to +2.9 as determined by Mössbauer spectroscopy. Summarizing both effects, t increases from 0.8965 to 0.8985.

Thus, the structural behavior of $Sr_2FeRe_{1-x}Sb_xO_6$ as a function of the Sb substitution grade can be analyzed as follows. For the undoped sample the room temperature structure is tetragonal. As the tolerance factor t remains essentially constant, a tetragonal structure is expected and observed for the Sb doping for the full range of substitution.

Figure 4 shows the experimental HRTEM image and the simulated high resolution transmission electron micrographs of $Sr_2FeRe_{0.1}Sb_{0.9}O_6$. The high resolution image [Fig. 4(a)] is in good agreement with the image of zone [1 0 −1] [Fig. 4(b)] simulated by the multislice method[23,24] (thickness of 504.27 Å, defocus −222 Å) using the CERIUS program suite.[25] The lattice spacings of 0.458 nm and 0.283 nm are in good agreement with (101) and (020) d-spacings of $Sr_2FeRe_{0.1}Sb_{0.9}O_6$.

The selected area electron diffraction (SAED) pattern of a $Sr_2FeRe_{0.1}Sb_{0.9}O_6$ particle of about 500 nm in diameter is given in Fig. 5(a). This is consistent with the kinematically calculated diffraction along [3 1 −3] [Fig. 5(b)] indicating the long range ordering of Fe, Re, and Sb within this particle.

B. Magnetic measurements

The magnetic susceptibility measurements of Sr_2FeReO_6 samples reveal spontaneous magnetization below T_C

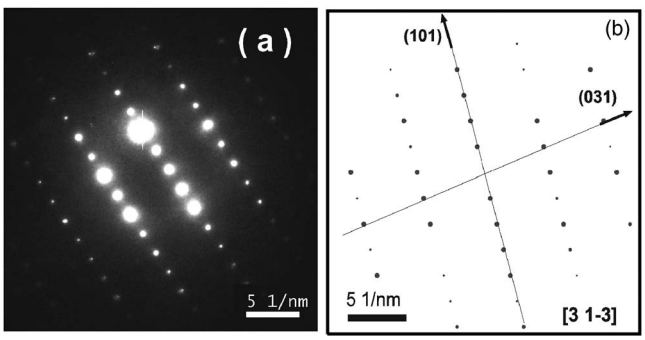

FIG. 5. (a) Selected area electron diffraction (SAED) pattern of $Sr_2FeRe_{0.1}Sb_{0.9}O_6$ and (b) dynamically calculated diffraction pattern of zone [3 1 −3].

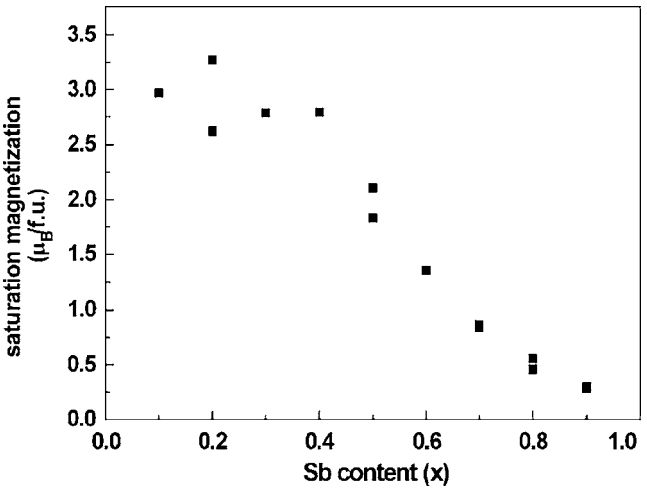

FIG. 6. Concentrational dependence of the saturation magnetization of $Sr_2FeRe_{1-x}Sb_xO_6$ ($0 \leqslant x \leqslant 0.9$) at 5 K.

=401(1) K. According to previous studies this compound can be considered a soft magnetic material. It contains ferromagnetically aligned magnetic moments of Fe atoms in the Fe sublattice and ferromagnetically aligned magnetic moments of Re atoms in the Re sublattice which leads to an overall ferrimagnetic behavior by superexchange via the oxygen atoms.[1,9–12,17] The superexchange pathways Fe-O-Re-O-Fe critically depend on the properties of the elements involved. A replacement of the Re atoms by a nonmagnetic, main group element with fixed valence such as Sb should have a dramatic influence on the superexchange pathways of the compound because of the lack of d orbitals of Sb. The concentrational dependence of the saturation magnetization of $Sr_2FeRe_{1-x}Sb_xO_6$ ($0 \leqslant x \leqslant 0.9$) at 5 K supports this assumption (Fig. 6). The saturation magnetizations were obtained by measuring hysteresis loops of all samples at 5 K [Fig. 7(b)].

As the concentration of Sb increases ($x > 0.6$) the saturation magnetization decreases and the susceptibility curves show a maximum corresponding to an antiferromagnetic type of ordering [Fig. 7(a)]. At a maximum Sb content of 90% the field dependence of the magnetization approaches a straight line and shows almost no hysteresis in comparison to the samples with higher Re concentration [Fig. 7(b)]. The results of the susceptibility measurements of Sb doped samples reveal ferrimagnetic behavior in the range of concentrations up to $x \cong 0.3$ as soon as the paramagnetic regions of the high-temperature magnetic susceptibility measurements could only be fitted by a ferrimagnetic model [Fig. 8(b)].

The compounds with 10%, 20%, and 30% of Sb order ferrimagnetically at T_C=388 K, 367 K, and 366 K, respectively [Fig. 8(b)]. Reciprocal susceptibilities of these samples in the paramagnetic regions were used to extract the parameters of magnetic interaction. Ferrimagnetic (T_C), paramagnetic (Θ_C), Curie temperatures, interaction parameter (μ) as well as Curie constants (C_A, C_B) for the two sublattices A and B for $Sr_2FeRe_{1-x}Sb_xO_6$ ($0.1 < x < 0.3$) were determined from the fit of the high-temperature magnetic susceptibility measurements [Fig. 8(b)]. The standard dependence describing

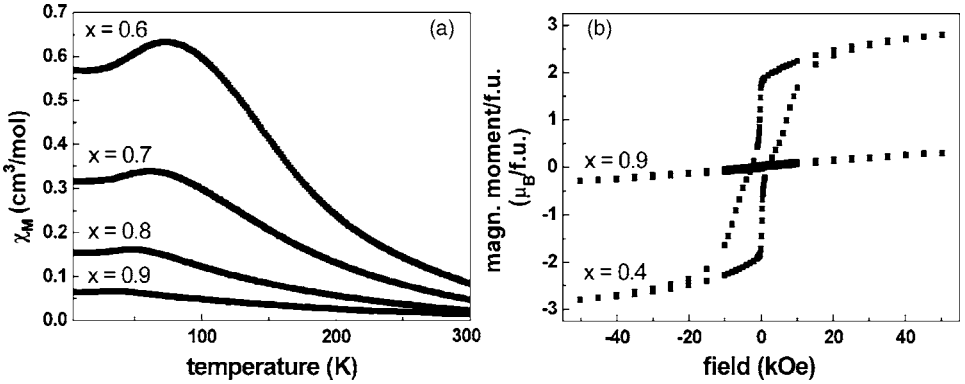

FIG. 7. (a) Molar susceptibility measured at 5 kOe in dc mode of $Sr_2FeRe_{1-x}Sb_xO_6$ and (b) field dependence of the magnetization of $Sr_2FeRe_{1-x}Sb_xO_6$ at 5 K.

the molar susceptibility χ_M in molecular field approximation has been applied,

$$\chi_M = \frac{(C_A + C_B)T - 2\mu C_A C_B}{T^2 - T_C^2}$$

with $T_C^2 = \mu^2 C_A C_B$ and

$$\Theta_C = -\frac{2\mu C_A C_B}{C_A + C_B}.$$

The fit in the paramagnetic region gives the following set of parameters for $Sr_2FeRe_{0.9}Sb_{0.1}O_6$: $\Theta_C = -169(6)$ K, $\mu = 173(8)$ mol cm^{-3}, $C_A = 9.5(3)$ cm^3 K mol^{-1}, and $C_B = 0.5(3)$ cm^3 K mol^{-1}. From the expression for the Curie constant $C = 0.125g^2S(S+1)$ with $g=2$ and the effective spin S, it follows that C_A is a Curie constant of the Fe based sublattice $[S(S+1)=19]$, whereas C_B can be attributed to the Re based sublattice $[S(S+1)=1]$.

Mössbauer data discussed hereafter indicate that only $Sr_2FeRe_{0.1}Sb_{0.9}O_6$ can be considered in terms of a "pure" antiferromagnetic phase from the microscopic point of view. The range of concentrations between $0.3 < x < 0.8$ can be considered an intermediate case, comprising antiferro- and ferrimagnetic-type of domains. The fit of the magnetic susceptibility data in this range of substitution qualitatively confirmed this model. It follows from the fit that the antiferromagnetic fraction increases as the Sb content increases. However, we found that the quantitative interpretation of the intermediate region is problematic because of unknown temperature dependence of ferri- and antiferromagnetic region fractions.

The temperature dependence of $\chi_M T$ [Fig. 8(a)] for $Sr_2FeRe_{0.1}Sb_{0.9}O_6$ shows ferromagnetic interactions above 150 K which changes to antiferromagnetic interaction for lower temperatures. Antiferromagnetic ordering occurs at $T_N = 36$ K. Magnetic susceptibility data for the 90% Sb doped sample were fitted using the expression for the magnetic susceptibility in the temperature range $40\ \text{K} < T < 130$ K corresponding to antiferromagnetic interactions: $\chi_M = \frac{C}{T-\Theta_N}$ with a paramagnetic Néel temperature $\Theta_N = \frac{1}{2}C(\alpha_{AA} + \alpha_{AB})$ and a Néel temperature $T_N = \frac{1}{2}C(\alpha_{AA} - \alpha_{AB})$. The constants $\alpha_{AA} = \alpha_{BB}$ and α_{AB} consider the exchange and dipole interactions within and between the sublattices A and B, respectively. The fit gives $\Theta_N = -96(2)$ K, $C = 9.3(1)$ cm^3 K mol^{-1}, $\alpha_{AA} = -6.4(1)$ mol cm^{-3}, and $\alpha_{AB} = -99.8(4)$ mol cm^{-3}. It is important to notice that the values of the Curie constants C and C_A for the Fe based sublattice are remarkably equal in both compounds. It means that a diamagnetic dilution of the Re sublattice only slightly perturbs the properties of the magnetic ions of the Fe based sublattice. In other words, the amount of magnetic centers and their local magnetic moments of the Fe based sublattice do not change significantly upon Sb substitution. Furthermore, one can conclude that Sb atoms do not replace Fe atoms and vice versa in antisiting fashion. These findings are in agreement with the structural results presented above as an essential antisite disorder -Fe-O-Fe- would lead to magnetic

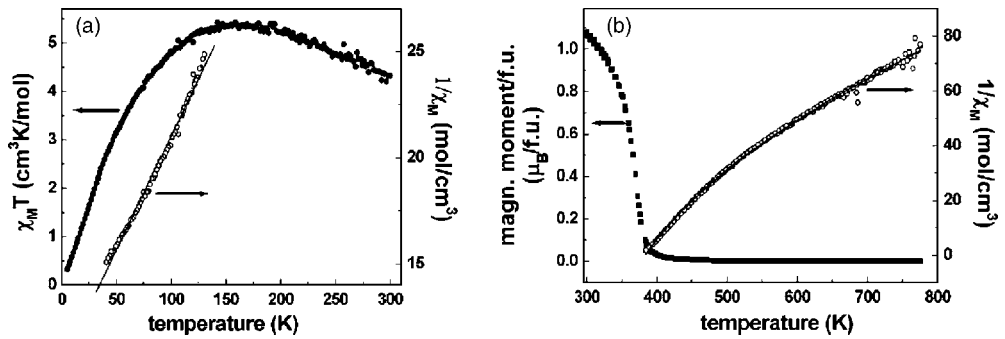

FIG. 8. (a) Molar susceptibility of $Sr_2FeRe_{0.1}Sb_{0.9}O_6$ multiplied by the temperature (•) and inverse molar susceptibility of $Sr_2FeRe_{0.1}Sb_{0.9}O_6$ (◦) versus temperature and (b) magnetization of $Sr_2FeRe_{0.9}Sb_{0.1}O_6$ (■) and inverse molar susceptibility of $Sr_2FeRe_{0.9}Sb_{0.1}O_6$ (◦) versus temperature.

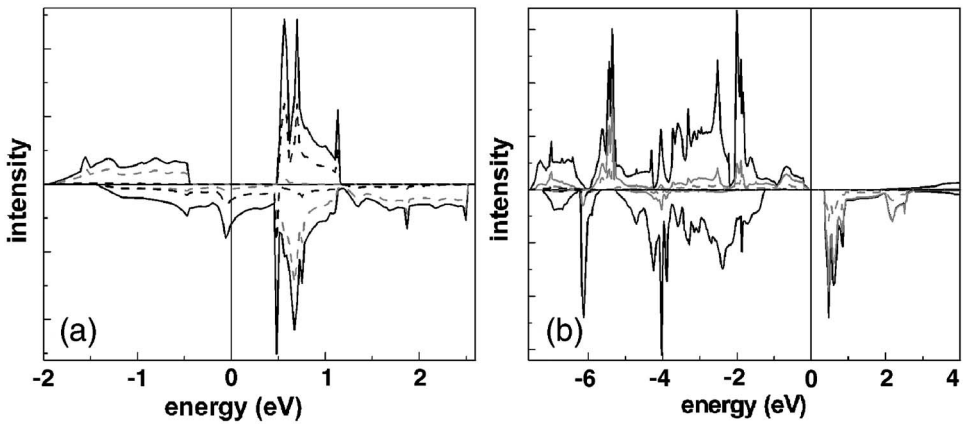

FIG. 9. Density of states of (a) Sr_2FeReO_6, in spin up direction: total DOS (solid black), partial DOS Fe *d* (grey dashed), Re *d* (black dashed); in spin down direction: total DOS (solid black), partial DOS Fe *d* (grey dashed), Re *d* (black dashed) and (b) Sr_2FeSbO_6, in spin up direction: total DOS (solid black), partial DOS Fe *d* e_g (grey dashed), Fe *d* t_{2g} (solid grey), Sb *p* (black dashed); in spin down direction: total DOS (solid black), partial DOS Fe *d* e_g (grey dashed), Fe *d* t_{2g} (solid grey), Sb *p* (black dashed).

moments for the two sublattices significantly different from the experimentally observed ones.

C. Band structure calculation

The double perovskite Sr_2FeReO_6 reveals half-metallic ferrimagnetic behavior at room temperature.[17] The conceptual basis for this behavior is a large density of states of one spin direction at the Fermi level E_F while the other spin direction is insulating [Fig. 9(a)]. Of the seven electrons which are distributed over the Fe and Re atoms five are fixed in Fe *d* orbitals in spin up direction whereas the Re *d* orbitals in this spin direction do not host electrons. The remaining two electrons are located in the Fe and Re *d* t_{2g} orbitals in spin down direction. The origin of the large density of states in the vicinity of the Fermi level can be related to a van Hove singularity in the band structure of these compounds as it was suggested in a previous study.[1,26] To investigate the influence of the diamagnetic dilution with a main group element on the Re sublattice, we have performed spin polarized *ab initio* band structure calculations for Sr_2FeSbO_6 using the WIEN2K software package.[16] The density of states given in Fig. 9(b) shows Sr_2FeSbO_6 to be a semiconductor or an insulator in spite of its spin polarization. The Fe *d* orbitals are completely filled in spin up direction whereas in spin down direction they do not contain any electrons. This situation corresponds to high spin Fe^{3+} ($3d^5$). In contrast, Sb does not show any significant participation to the DOS near E_F as expected from its lack of *d* orbitals. Therefore one can expect a fixed valence for antimony (Sb^{5+}). Finally, Sb doping "switches off" the itinerant magnetism of the parent compound.

D. Conductivity measurements

The results of the conductivity measurement of four selected samples ($Sr_2FeRe_{1-x}Sb_xO_6$, $x=0$, 0.1, 0.4, 0.6) are presented in Fig. 10. In accordance with previous results[17] the undoped sample reveals a metallic behavior in the whole temperature range. In contrast, Sb doped samples are semiconducting. The room temperature resistance of the sample with highest doping level of 60% Sb is several orders of magnitude higher than that of the undoped one and it becomes almost insulating upon cooling in agreement with band structure calculations.

E. Mössbauer spectroscopy

^{57}Fe and ^{121}Sb Mössbauer experiments give deeper insight into the magnetic structure of $Sr_2FeRe_{1-x}Sb_xO_6$. In the original ferrimagnetically ordered, undoped Sr_2FeReO_6, local magnetic moments of iron atoms are aligned in parallel. Mössbauer spectra reveal only one Fe site with a hyperfine magnetic field of 468.6(5) kOe at 44.2 K [Fig. 11(a)]. The 6-line pattern of the spectra is typical for materials in the magnetically ordered phase and the very sharp lines are indicative of a very high degree of Fe-Re(Sb) order in the structure. A considerable cationic disorder would result in additional (broadened) spectral lines due to a distribution of different environments of iron [Fig. 11(a)]. Measurements on

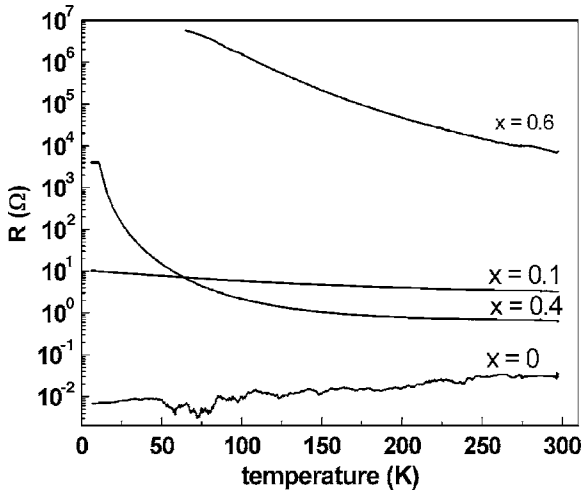

FIG. 10. Conductivity measurements without application of an external magnetic field of $Sr_2FeRe_{1-x}Sb_xO_6$.

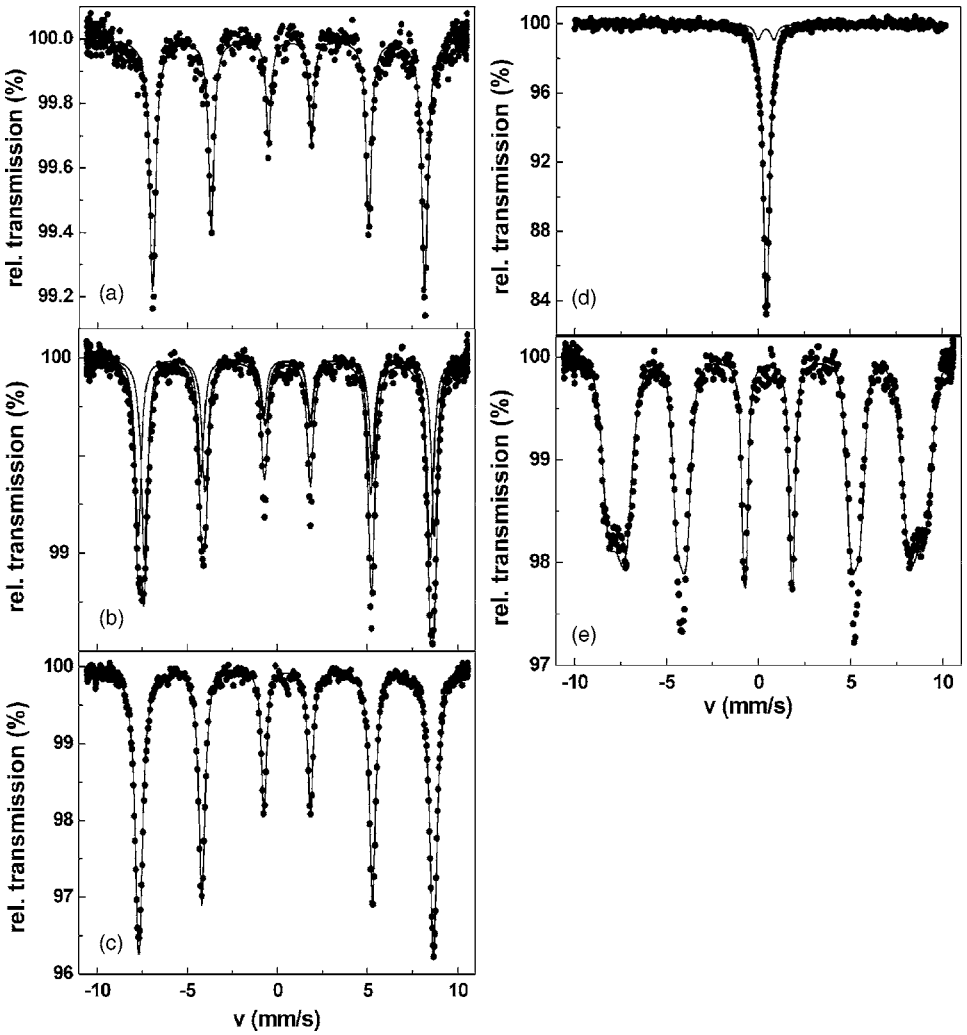

FIG. 11. ^{57}Fe Mössbauer spectra of (a) Sr_2FeReO_6 (4.2 K), (b) $Sr_2FeRe_{0.4}Sb_{0.6}O_6$ (4.2 K), (c) $Sr_2FeRe_{0.1}Sb_{0.9}O_6$ (4.2 K), (d) $Sr_2FeRe_{0.1}Sb_{0.9}O_6$ (300 K), and (e) $Sr_2FeRe_{0.1}Sb_{0.9}O_6$ (4.2 K) in an external magnetic field of 50 kOe.

Sr_2FeReO_6 in an external magnetic field of 50 kOe at 4.2 K show a decrease of the hyperfine magnetic field to 421(2) kOe which clearly indicates a ferromagnetic type of ordering within the Fe sublattice. 10%–80% of Sb doping leads to at least two Fe sites which can be seen from the line splitting in the Mössbauer spectra [Fig. 11(b)]. As follows from the magnetic susceptibility measurements, the transformation from ferri- to antiferromagnetic type of ordering occurs in this range of concentrations. In contrast, the spectra of $Sr_2FeRe_{0.1}Sb_{0.9}O_6$ at room temperature and 4.2 K exhibit only one crystallographic Fe position with a hyperfine magnetic field of 506.8(2) kOe [Figs. 11(c) and 11(d)]. The application of an external magnetic field of 50 kOe causes splitting of the Mössbauer spectrum into two subspectra with hyperfine magnetic fields of 481(4) and 533(4) kOe [Fig. 11(e)]. This fact indicates an antiferromagnetic arrangement of the Fe cations and confirms the antiferromagnetic ordering found in the magnetic susceptibility measurements. However, as one can judge from the non satisfactory fit of the Mössbauer spectra taken in an external magnetic field, the magnetic structure could be even more complex. From Mössbauer studies on samples with an intermediate degree of Sb doping (30%–80%) in an external magnetic field one can conclude that different types of magnetic clusters either ferri- or antiferromagnetic coexist.

The ^{121}Sb Mössbauer spectroscopic study at 4.2 K exhibits paramagnetic spectra with an isomer shift δ(Sb) $=0.20(5)$ mm s^{-1} for the total range of Sb concentration (Fig. 12). This isomer shift indicates a 5+ Sb valence state. The spectra of compounds with an intermediate Sb content are slightly more broadened in comparison to those of the nondoped and 90% doped samples, which is in agreement with the presence of ferri- and antiferromagnetic domains as discussed above.

A general advantage of ^{121}Sb Mössbauer spectroscopy is the high sensitivity of the isomer shift on the Sb valence state. The fact that the isomer shift of Sb is constant for the total range of concentrations is remarkable because Sb^{5+} substitutes Re atoms with valence states varying from +5 to +6. From a study of the $Sr_2Fe_{1-x}Zn_xReO_6$ and $Sr_2Fe_{1-x}Cr_xReO_6$ series we concluded that the iron valence state is constant over the whole doping series whereas the Re atoms can be considered as a redox buffer with a valence state depending on the doping level.[1] Following this idea, we can conclude that the valence state of the iron atoms should be concentrationally dependent. In other words, iron atoms must play the role of a redox buffer.

The average Fe valence state for $Sr_2FeRe_{0.1}Sb_{0.9}O_6$ can be estimated by comparing the isomer shift of $Sr_2FeRe_{1-x}Sb_xO_6$ ($x=0$ and $x=0.9$) with the isomer shifts of standard reference

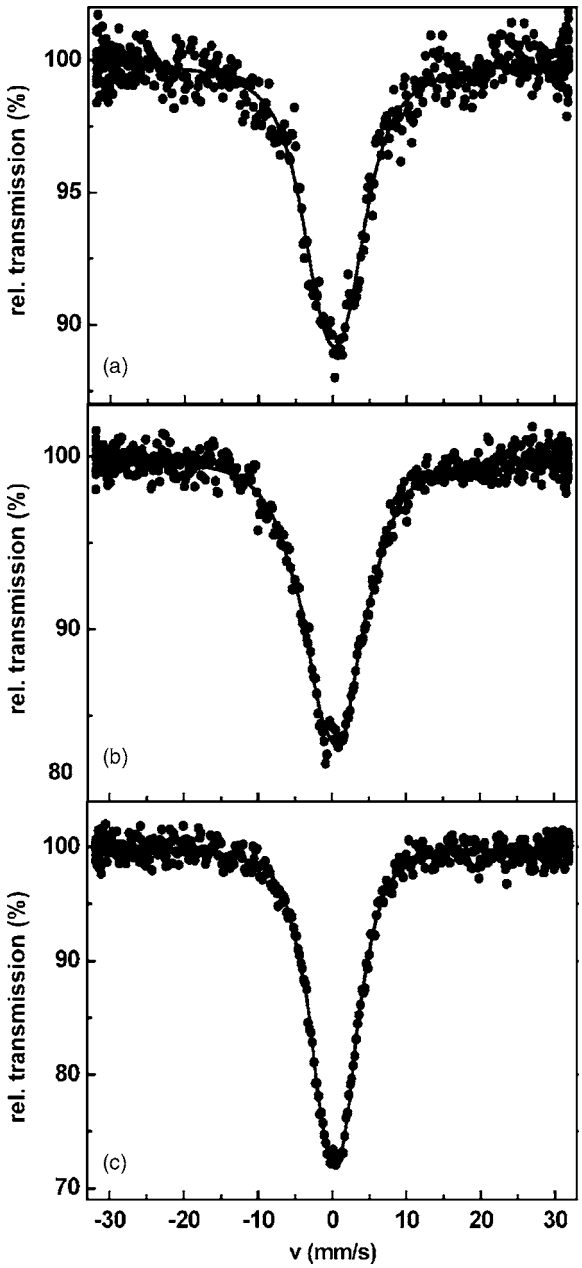

FIG. 12. ^{121}Sb Mössbauer spectra measured at 4.2 K of (a) $Sr_2FeRe_{0.9}Sb_{0.1}O_6$, (b) $Sr_2FeRe_{0.4}Sb_{0.6}O_6$, and (c) $Sr_2FeRe_{0.1}Sb_{0.9}O_6$.

compounds $Cs_2Fe_2^{2+}(MoO_4)_3$ and $Li_3Fe^{3+}(MoO_4)_3$ using the same procedure as described previously.[1] From the values of the isomer shifts $\delta(\mathrm{Fe}, x=0.9)=0.504(5)$ mm s^{-1} and $\delta(\mathrm{Fe}, x=0)=0.670(5)$ mm s^{-1} it follows that the valence state of Fe is 2.9+. This is in good agreement with the Sb^{5+} valence state following from the chemical composition of the 90% Sb doped sample $Sr_2Fe^{2.9+}Re^{6+}_{0.1}Sb^{5+}_{0.9}O_6$.

The concentrational dependence of the isomer shifts and hyperfine magnetic fields of iron atoms in both types of clusters (ferri-, antiferro-) is shown in Fig. 13. Both values strongly depend on the Sb concentration. Average values of the isomer shifts and hyperfine magnetic fields exhibit an almost linear concentrational dependency. This linear correlation indicates that (i) the samples are chemically and structurally homogeneous and (ii) ferri- and antiferromagnetic clusters coexist within the same crystal structure.

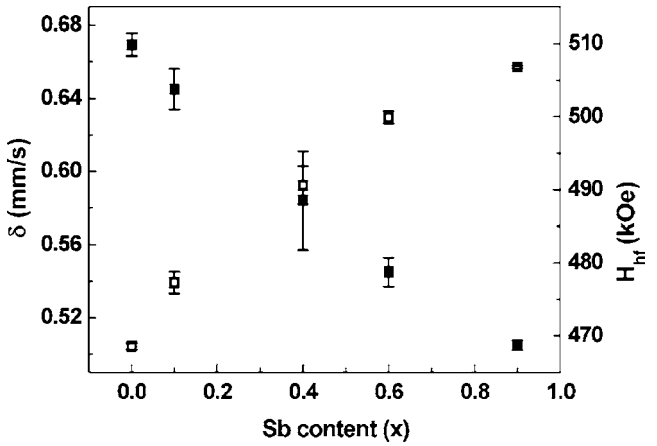

FIG. 13. Isomer shifts δ (■) and hyperfine magnetic fields H_{hf} (□) of the Fe atoms as a function of the Sb content.

IV. CONCLUSION

The interpretation of the magnetic structure of the compounds under study follows from the crystal structure determination, magnetic characterization, band structure calculations, conductivity measurements, and Mössbauer experiments. Ferromagnetic alignment of the magnetic moments of the Fe atoms in the Fe sublattice and the Re atoms in the Re sublattice of Sr_2FeReO_6 is mediated by superexchange via oxygen atoms leading to an overall ferrimagnetic behavior. This situation is valid up to a replacement level of 30% of Sb for Re as shown at a microscopic level by Mössbauer spectroscopy and at a macroscopic level by magnetic susceptibility measurements. In contrast, large Sb contents lead to antiferromagnetic behavior. X-ray diffraction and Mössbauer spectroscopy studies revealed the absence of

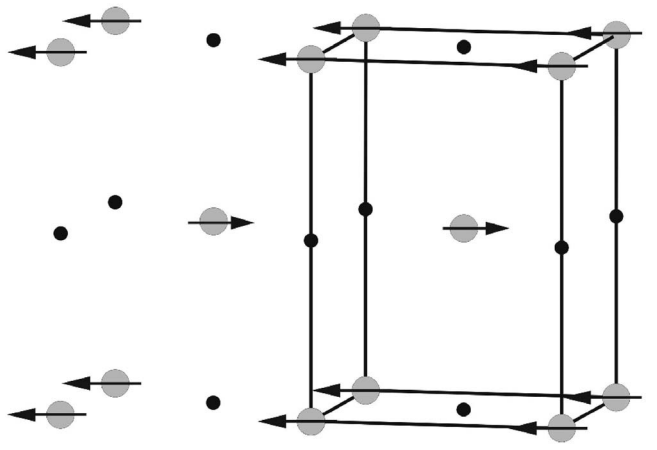

FIG. 14. Magnetic structure of Sr_2FeSbO_6 based on neutron diffraction studies by Cussen *et al.* (Ref. 27). Within the tetragonal unit cell, only M (Fe, grey) and M' (Sb, black) positions are shown.

Fe/Re antisite disorder. This supports a superexchange via -Fe-O-Re-O-Fe- which requires an ordered arrangement of Fe and Re/Sb on their respective lattice sites. The substitution of Re by Sb destroys the itinerant magnetism as Sb (i) is lacking *d* orbitals involved in states at the Fermi level, (ii) shows no magnetic splitting in the Mössbauer spectra, and (iii) carries no magnetic moment according to the results of a neutron diffraction study by Cussen *et al.*[27] (Fig. 14). At the moment, we cannot ultimately conclude whether Sb atoms take part instead of Re atoms in the superexchange pathway -Fe-O-Sb-O- Fe or alternatively the antiferromagnetic order is determined by direct Fe-Fe exchange. Cussen *et al.*[27] suggested a model of magnetic interaction which is in agreement with the experimental findings of the present work. Although the Fe-Fe separations of about 4 Å in the title compounds are fairly large, a case of ferromagnetic exchange between layers containing transition elements over distances of about 40 Å has been reported,[28] lends support to the idea of direct ferromagnetic exchange between the Fe atoms in the double perovskites $Sr_2FeRe_{1-x}Sb_xO_6$ $(0.6<x<0.9)$.

ACKNOWLEDGMENTS

This work was supported by the Deutsche Forschungsgemeinschaft (Forschergruppe 559) and the Materials Science Center (MWFZ) at the Johannes-Gutenberg Universität Mainz. We are indebted to F. Emmerling (Bundesanstalt für Materialforschung und -prüfung, I.3 AG Röntgenstrukturanalytik) for acquiring x-ray powder data.

[1] A. Jung, I. Bonn, V. Ksenofontov, G. Melnyk, J. Ensling, C. Felser, and W. Tremel, J. Mater. Chem. **15**, 1760 (2005).
[2] A. I. Smirnov, V. N. Glazkov, H.-A. Krug von Nidda, A. Loidl, L. N. Demianets, and A. Ya. Shapirov, Phys. Rev. B **65**, 174422 (2002).
[3] X. Chen, Ch. Binek, A. Hochstrat, and W. Kleemann, Phys. Rev. B **65**, 012415 (2001).
[4] P. Hansen and K. Witter, Phys. Rev. B **27**, 1498 (1983).
[5] Ch. Binek, W. Kleemann, and D. P. Belanger, Phys. Rev. B **57**, 7791 (1998).
[6] J. Longo and R. Ward, J. Am. Chem. Soc. **83**, 2816 (1961).
[7] A. W. Sleight, J. Longo, and R. Ward, Inorg. Chem. **1**, 245 (1962).
[8] O. Chmaissem, R. Kruk, B. Dabrowski, D. E. Brown, X. Xiong, S. Kolesnik, J. D. Jorgensen, and C. W. Kimball, Phys. Rev. B **62**, 14197 (2000).
[9] H. Kato, T. Okuda, Y. Okimoto, Y. Tomioka, K. Oikawa, T. Kamiyama, and Y. Tokura, Phys. Rev. B **65**, 144404 (2002).
[10] S. Nakamura, M. Tanaka, H. Kato, and Y. Tokura, J. Phys. Soc. Jpn. **72**, 424 (2003).
[11] E. Carvajal, O. Navarro, R. Allub, M. Avignon, and B. Alascio, Phys. Status Solidi B **242**, 1942 (2005).
[12] A. Poddar and S. Das, Physica B **344**, 325 (2004).
[13] W. Haberditzl, *Magnetochemie* (Akademie-Verlag, Berlin, 1968).
[14] K. Lagarec and D. G. Rancourt, Nucl. Instrum. Methods Phys. Res. B **129**, 266 (1997).
[15] H. Spiering, L. Deák, and L. Bottyán, Hyperfine Interact. **125**, 197 (2000).
[16] P. Blaha, K. Schwarz, G. K. H. Madsen, D. Kvasnicka, and J. Luitz, *Wien2k, An Augmented Plane Wave + Local Orbitals Program for Calculating Crystal Properties* (Karlheinz Schwarz, Techn. Universtität Wien, Austria, 2001).
[17] K.-I. Kobayashi, T. Kimura, Y. Tomioka, H. Sawada, K. Terakura, and Y. Tokura, Phys. Rev. B **59**, 11159 (1999).
[18] T. H. Kim, M. Uehara, S.-W. Cheong, and S. Lee, Appl. Phys. Lett. **74**, 1737 (1999).
[19] J. Rodríguez-Carvajal, Physica B **192**, 55 (1993).
[20] R. D. Shannon, Acta Crystallogr., Sect. A: Cryst. Phys., Diffr., Theor. Gen. Crystallogr. **32**, 751 (1976).
[21] U. Müller, *Anorganische Strukturchemie* (Teubner Studienbücher, Stuttgart, 1996).
[22] G. Popov, M. Greenblatt, and M. Croft, Phys. Rev. B **67**, 024406 (2003).
[23] J. M. Cowley and A. F. Moodie, Acta Crystallogr. **10**, 609 (1957).
[24] W. O. Saxton, M. A. O'Keefe, D. J.H. Cockayne, and M. Wilkens, Ultramicroscopy **12**, 75 (1983).
[25] CERIUS2 version 4.6MS, Molecular modeling environment from Accelrys Inc. 9685 Scranton Road, San Diego, CA 92121-3752.
[26] C. Felser, R. Seshadri, A. Leist, and W. Tremel, J. Mater. Chem. **8**, 787 (1998).
[27] E. J. Cussen, J. F. Vente, P. D. Battle, and T. C. Gibb, J. Mater. Chem. **7**, 459 (1997).
[28] M. Drillon, P. Panissod, P. Rabu, J. Souletie, V. Ksenofontov, and P. Gütlich, Phys. Rev. B **65**, 104404 (2002).